Collision-induced transitions between the Zeeman-split (J,m) levels of Rb($5\,^2P_{1/2}$, $5\,^2P_{3/2}$)

Matthew D. Rotondaro* and Glen P. Perram†
Department of Engineering Physics, Air Force Institute of Technology, 2950 P Street, Building 640, Wright-Patterson Air Force Base, Ohio 45433-7765
(Received 29 December 1997)

The collisional dynamics of the Zeeman-split levels of Rb($5\,^2P_{1/2}$, $5\,^2P_{3/2}$) has been studied in the presence of a strong magnetic field (1.65 T) using steady-state, spectrally resolved laser-induced fluorescence techniques. State-to-state cross sections for transitions between (J,m) levels ranged from 1.6×10^{-15} to 2.5×10^{-14} cm^2 for collisions with nitrogen and rare gases. The cross sections indicate a significant dependence on (J,m) states and certain symmetry relations such as $\sigma(J,m\rightarrow J,m')=\sigma(J,-m\rightarrow J,-m')$ and $\sigma(J,m\rightarrow J,'m)=\sigma(J,-m\rightarrow J',-m)$ are demonstrated. The results also agree favorably with theoretical predictions of the relative decay rates for orientation, alignment, and octupole moment. The cross sections for rare-gas collision partners scale with polarizability as predicted. [S1050-2947(98)02709-7]

PACS number(s): 34.30.+h

I. INTRODUCTION

The collisional dynamics of Zeeman split sublevels of the excited ^2P states of alkali metals has been studied extensively [1,2] primarily using optical depolarization and Hanle-effect techniques [3–13] and, to a lesser degree, via fluorescence monitoring of individual (J,m) populations [14–21]. The depolarization techniques do not provide a unique description of the state-to-state transition rates for the complete $^2P_{3/2}$ manifold [14–16]. Usually, certain symmetry relationships [17,20] between the state-selective cross sections are employed to reduce the number of independent $\sigma(J,m\rightarrow J',m')$ cross sections to be determined.

The fluorescence monitoring of all the individual $^2P_{J,m}$ populations can provide a complete determination of the $\sigma(J,m\rightarrow J',m')$ cross sections [14,15], but requires strong magnetic fields and high spectral resolution. For example, the Zeeman splitting of the Rb($^2P_{3/2}$) levels for a 2-T magnetic field is B $\mu_B g_{3/2}=1.3\,\mathrm{cm}^{-1}$. Since the fine-structure splitting of Rb($5\,^2P$) is moderate, $237.6\,\mathrm{cm}^{-1}$, transitions between the $^2P_{1/2}$ and $^2P_{3/2}$ states induced by rare gases are relatively slow. However, collisional transfer between these fine-structure levels for molecular collision partners is relatively rapid [22] and the collisional manifold includes all six Zeeman substates. By optically pumping each $^2P_{J,m}$ state (the parent state) and monitoring the fluorescence from all the resulting collisionally populated $^2P_{J',m'}$ states (the satellite states) as a function of buffer gas pressure, the complete set of $\sigma(J,m\rightarrow J',m')$ cross sections is determined. Such fluorescence monitoring studies have been performed for Na($3\,^2P$) [14,15], K($4\,^2P$,$5\,^2P$) [16–19], and Rb($6\,^2P$) [20] collisions with rare gases. The dependence of the helium collision cross section on magnetic field strength for the pair of Rb($5\,^2P_{1/2}$) substates has also been examined [21]. The current work provides the cross sections for the six Zeeman substates of Rb($5\,^2P_{1/2,3/2}$) upon collision with N_2, He, Ne, Ar, Kr, and Xe for a magnetic field of 1.65 T and is analyzed to verify symmetry and scaling predictions.

The spectroscopy and collisional processes for ^{87}Rb are illustrated in Fig. 1. The fine-structure splitting is $237.6\,\mathrm{cm}^{-1}$ and produces the two prominent D_1 and D_2 lines near $\lambda=794.7$ nm and $\lambda=780.0$ nm, respectively. Transfer between these two ^2P_J states has been studied extensively for a variety of collision partners [22–24]. The hyperfine structure is also well characterized [2] and the splittings are indicated in Fig. 1. In the presence of a magnetic field, the m degeneracy of the J states is removed and the strong field (1.65 T) limit is shown on the right-hand side of Fig. 1. Also indicated are typical kinetic processes, including collisional transitions between Zeeman-split substates, $\sigma(J,m\rightarrow J,m')$, collisional transitions between fine-structure levels, $\sigma(J,m\rightarrow J',m')$, collisional quenching of the ^2P manifold, $\sigma_q(^2P_{J,m}\rightarrow{}^2S)$, and spontaneous radiative transitions, $A(^2P_{J,m}\rightarrow{}^2S_{1/2,m'})$. The spontaneous emission rates for the

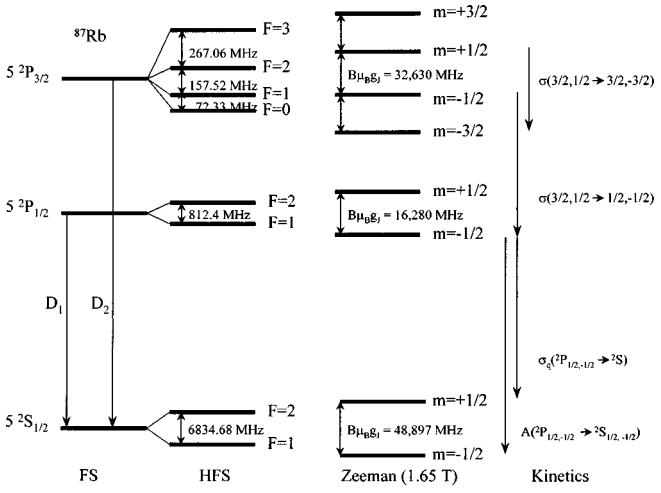

FIG. 1. Energy-level diagram for ^{87}Rb, indicating fine-structure (FS), hyperfine structure (HFS), and Zeeman splitting in a 1.65-T magnetic field.

*Present address: Laser Devices Division, Phillips Laboratory, PL/LID, Kirtland AFB, NM 87117-6008.
†Author to whom correspondence should be addressed. FAX: (937)-255-2921. Electronic address: gperram@afit.af.mil

TABLE I. Theoretical line strengths, f, for ${}^2P_{J,m} \rightarrow {}^2S_{1/2,m}$ [26].

(J,m)	${}^2P_{J,m} \rightarrow {}^2S_{1/2,+1/2}$	${}^2P_{J,m} \rightarrow {}^2S_{1/2-1/2}$
${}^2P_{1/2,+1/2}$	4	4
${}^2P_{1/2,11/2}$	4	4
${}^2P_{3/2,+3/2}$	6	
${}^2P_{3/2,+1/2}$	8	2
${}^2P_{3/2,-1/2}$	2	8
${}^2P_{3/2,-3/2}$		6

D_1 and D_2 lines are 3.70×10^7 s^{-1} and 3.56×10^7 s^{-1}, respectively [25] and the theoretical line strengths are provided in Table I [26].

II. EXPERIMENTAL APPARATUS

The experimental apparatus for measuring the cross sections for collision-induced transfer between the Zeeman-split levels is depicted schematically in Fig. 2. A Spectra-Physics 15 W argon ion laser was used to pump a tunable Coherent 899 Ti:sapphire ring laser. The ring laser power was limited to less than 100 mW to avoid saturation effects [27]. The ring laser has a frequency stability and linewidth of $\sim$0.5 MHz. The rubidium cell has been described in detail previously [22,35] and consisted of a rectangular glass fluorocell with a 1-cm and a 2-cm path length maintained at a temperature of $T=330$ K. The laser beam was positioned 1–2 mm from the fluorescence observation window, ensuring no optical trapping for typical Rb concentrations of about 10^{-7} torr [22,35]. The cell and a rubidium break-seal ampule (99.8% pure with naturally occurring isotopic concentrations) was blown onto a glass valve. The addition of N_2 and rare gases (>99.99% purity) was controlled by a precision variable leak valve. Buffer gas pressure changes of up to 10 torr were measured with an accuracy of better than 1 mtorr with an MKS model 390 capacitance manometer.

The laser was tuned to one of the six allowed ($\Delta m=0, \pm1$) ${}^2S_{1/2,m'}$-${}^2P_{J,m}$ transitions and the resulting fluorescence was coupled into a 1.3-m monochromator and monitored via a thermoelectrically cooled RCA C31034A-02 photomultiplier tube and photon counting system. The resolution at $\lambda=780$ nm was $\Delta\lambda=0.012$ nm, which is sufficient to resolve each peak in the spectrum. The magnetic field was produced by a Lake Shore electro-magnet. The magnet's poles were 2.54 cm in diameter and the separation was 2 cm. The magnetic field uniformity is better than 10% of the central field within a diameter of 2.5 cm. The magnet was operated at 80 A, which resulted in a field strength of 1.65 T.

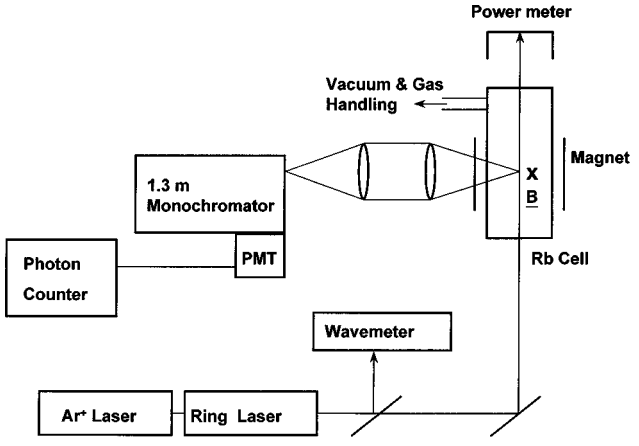

FIG. 2. Spectrally resolved laser-induced fluorescence apparatus.

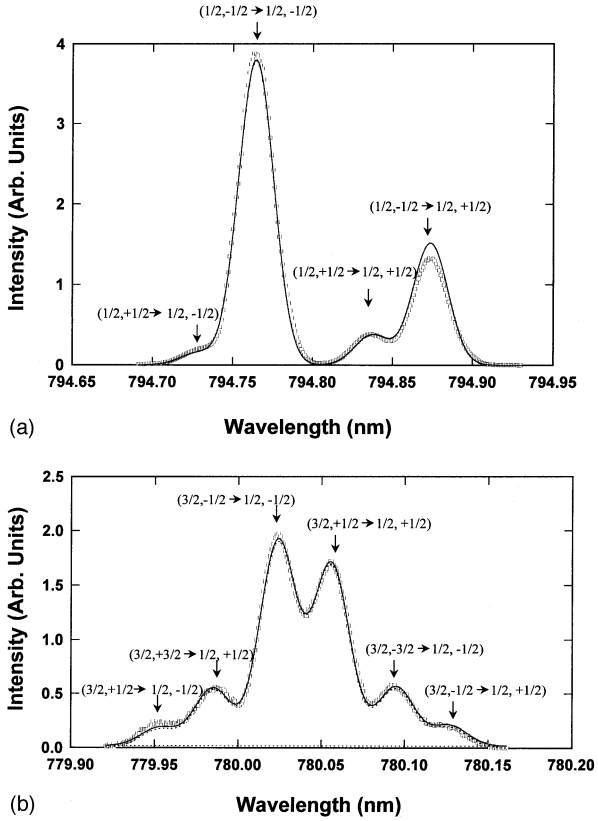

FIG. 3. Emission from (a) Rb ($5\,{}^2P_{1/2,m}$) and from (b) Rb ($5\,{}^2P_{3/2,m}$) after laser excitation of the ${}^2S_{1/2,-1/2} \rightarrow {}^2P_{1/2,-1/2}$ transition for a nitrogen buffer gas pressure of 1.2 Torr. The spectrally resolved emission (□) and a fit of the synthetic spectra of Eq. (1) (—) are shown in both plots. The peaks are labeled ($J',m' \rightarrow J'',m''$) for emission transitions ${}^2P_{J',m'} \rightarrow {}^2S_{J'',m''}$. The spectra are consistent with a magnetic field of 1.65 T.

Scattered laser light transmitted through the monochromator at the parent wavelength was small, typically <15%. Temporarily turning the magnetic field off shifts the absorption feature away from the laser wavelength and allows for correction to the spectrum for the effect of scattered light [27]. Total fluorescence was also detected to monitor the stability of laser power and frequency.

III. RESULTS

The resolved fluorescence after laser excitation of Rb ${}^2S_{1/2,-1/2} \rightarrow {}^2P_{1/2,-1/2}$ for 1.2 Torr of nitrogen buffer gas is shown in Fig. 3. The emission from the laser pumped ${}^2P_{1/2,m}$ manifold [Fig. 3(a)] indicates two prominent spectral features arising from transitions between the parent state to the pair of Zeeman-split ground states, ${}^2P_{1/2,-1/2} \rightarrow {}^2S_{1/2,-1/2}$ and ${}^2P_{1/2,-1/2} \rightarrow {}^2S_{1/2,1/2}$, and two weaker satellite lines due to emission from the collisionally populated ${}^2P_{1/2,1/2}$ state. The theoretical line strengths of the two lines from the parent state are equal, and the observed relative

intensities reflect a polarization dependence on the transmission of the grating monochromator, as discussed below. Variations of up to 10% in the relative detectivities were sometimes observed, as shown by the deviation from fit and observed spectra in Fig. 3(a). The spectrum shown in Fig. 3(b) indicates a significant probability for collisional transfer to the $^2P_{3/2}$ manifold as well. In this case, six optically allowed transitions, $\Delta m = 0, \pm 1$, from $^2P_{3/2,m}$ to $^2S_{1/2,m'}$ are observed. The two strongest features involve $\Delta m = 0$.

To accurately determine the relative populations within the $^2P_{J,m}$ manifold from the spectra of Fig. 3, we fit simulated spectra to the observed spectra. Figure 3 also shows a simulated spectrum based on a convolution of Gaussian peaks:

$$I(\lambda) = I_0 + \sum_{i=1}^{n} I_i g(\lambda;\lambda_i,\Delta\lambda), \tag{1}$$

where I_0 is the constant baseline signal, $g(\lambda;\lambda_i,\Delta\lambda)$ is the Gaussian line shape,

$$\left(\frac{4\ln 2}{\pi}\right)^{1/2}\left(\frac{\lambda_i^2}{c\Delta\lambda}\right)\exp\left[-4\ln 2\left(\frac{\lambda_i(\lambda_i-\lambda)}{\lambda\Delta\lambda}\right)\right],$$

I_i is the intensity of the ith spectral line$= f_i d_i N(^2P_{J,m})_i$, d_i is the relative detectivity for the ith spectral line (linear or circular polarization), f_i is the line strength ith spectral line, as given in Table I, $N(^2P_{J,m})_i$ is the population of the emitting state corresponding to the ith spectral line, λ_i is the line center of the ith spectral line, $\Delta\lambda$ is the linewidth [full width at half maximum (FWHM)], common to each line, and $n = 4$ or 6, for the $^2P_{1/2}$ or $^2P_{3/2}$ manifold, respectively.

The line positions, λ_i, particularly their separations, are determined by the magnetic field strength B. Thus, the line positions may be defined by a single fit parameter. The linewidth $\Delta\lambda$ is instrumentally limited and common for each spectral line. The ratio of detectivities for linear and circularly polarized light was determined independently as $d_{\rm pol} = 2.5$ [27] and the spectral fits were constrained to this value. Therefore, the fit parameters for the spectral simulation are (1) the populations of the emitting levels, $N(^2P_{J,m})$, (2) the linewidth $\Delta\lambda$, (3) the magnetic field strength B, and (4) a constant baseline I_0.

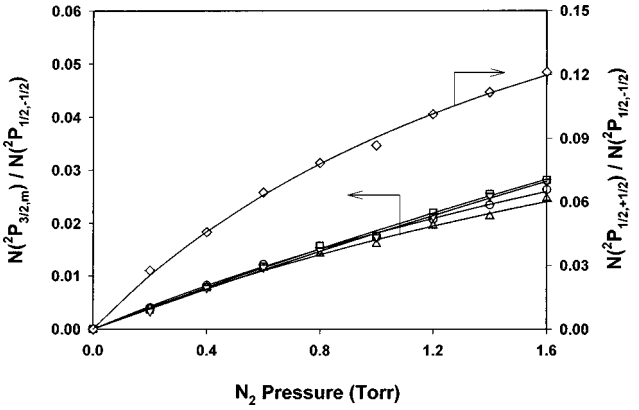

FIG. 4. Population in the satellite levels: ($\diamond$) $^2P_{1/2,1/2}$, ($\bigcirc$) $^2P_{3/2,3/2}$, ($\triangle$) $^2P_{3/2,1/2}$, ($\square$) $^2P_{3/2,-1/2}$, and ($\triangledown$) $^2P_{3/2,-3/2}$, relative to the population in the parent, $^2P_{1/2,-1/2}$, level as a function of nitrogen buffer gas pressure. A least-square fit of the data (—) to Eq. (8) is shown for each satellite level. The population in the $^2P_{1/2,1/2}$ level is considerably larger than the populations in the $^2P_{3/2,m}$ manifold, and a secondary scale for the y axis is provided for the ($\diamond$) $^2P_{1/2,1/2}$ level.

The population in the satellite levels after excitation of the $^2S_{1/2,-1/2} \rightarrow {}^2P_{1/2,-1/2}$ transition is shown as a function of nitrogen pressure in Fig. 4. Note that the probability of transition to the $^2P_{3/2}$ manifold is somewhat less than that for the transition to the other Zeeman-split substate within the pumped $^2P_{1/2}$ manifold. Similar data were recorded after laser excitation of each $^2P_{J,m}$ state. To extract the transition rates from the data of Fig. 4, the kinetic mechanism as shown in Fig. 1 is analyzed:

$$\mathrm{Rb}(^2S_{1/2}) + h\nu_p \rightarrow \mathrm{Rb}(^2P_{J,m}), \tag{2}$$

$$\mathrm{Rb}(^2P_{J,m}) + M \rightarrow \mathrm{Rb}(^2P_{J',m'}), \tag{3}$$

$$\mathrm{Rb}(^2P_{J,m}) + M \rightarrow \mathrm{Rb}(^2S_{1/2}), \tag{4}$$

$$\mathrm{Rb}(^2P_{J,m}) \rightarrow \mathrm{Rb}(^2S_{1/2}) + h\nu, \tag{5}$$

where $^2P_{J,m}$ denotes the laser prepared parent state, $^2P_{J',m'}$ denotes the collisionally populated state monitored by fluorescence, and $M = \mathrm{N_2}$, He, Ne, Ar, Kr, or Xe. The rate of populating a satellite level is

$$\frac{d[\mathrm{Rb}(^2P_{J',m'})]}{dt} = k_j[\mathrm{Rb}(^2P_{J,m})][M] - \left\{k_5 + k_4[M] + \sum_{J'',m''} k_3(J',m' \rightarrow J'',m'')[M]\right\}[\mathrm{Rb}(^2P_{J',m'})]$$
$$+ \left\{\sum_{J'',m'' \neq J,m} k_3(J'',m'' \rightarrow J',m')[M]\right\}[\mathrm{Rb}(^2P_{J'',m''})] \tag{6}$$

where the rate coefficients are related to the cross sections of Fig. 1 by

$$k_3(J,m \rightarrow J',m) = \sigma(J,m \rightarrow J',m')g, \quad k_4(J,m) = \sigma_q(^2P_{J,m} \rightarrow {}^2S)g,$$

$$k_5(J,m) = A(^2P_{J,m} \rightarrow {}^2S),$$

$$g = \sqrt{8k_BT/\pi\mu},$$

where g is the relative collision speed. Solving Eq. (6) under steady-state excitation conditions yields

TABLE II. Cross sections for transitions between Zeeman-split Rb($^2P_{J,m}$) Levels induced by collisions with N_2, $\sigma(J,m\rightarrow J',m')$ (10^{-16} cm^2).

(J,m)	$(J',m')=$ (3/2,+3/2)	$(J',m')=$ (3/2,+1/2)	$(J',m')=$ (3/2,−1/2)	$(J',m')=$ (3/2,−3/2)	$(J',m')=$ (1/2,+1/2)	$(J',m')=$ (1/2,−1/2)
(3/2,+3/2)		75 ±9	57 ±8	37 ±4		
(3/2,+1/2)	90 ±5		59 ±2	73 ±7	15±2	14±1
(3/2,−1/2)	71 ±5	61 ±2		82 ±6	13±1	15±1
(3/2,−3/2)	40 ±8	52 ±6	66 ±6			
(1/2,+1/2)	4.7±0.3	5.0±0.2	5.2±0.1	5.5±0.2		32±3
(1/2,−1/2)	5.4±0.2	5.1±0.2	4.9±0.2	4.7±0.2	33±1	

$$\frac{N(^2P_{J',m'})}{N(^2P_{J,m})}=\frac{\sigma(J,m\rightarrow J',m')g[M]}{A(^2P_{J,m}\rightarrow{}^2S)+\left\{\sigma_q(J',m')+\sum_{J'',m''}\sigma(J',m'\rightarrow J'',m'')-\sum_{J'',m''\neq J,m}\sigma(J'',m''\rightarrow J',m')\,\frac{N(^2P_{J'',m''})}{N(^2P_{J,m})}\right\}g[M]}. \tag{7}$$

The last term in the denominator represents multiple collisions that populate the observed level other than directly from the parent state. Such processes are negligible at low pressures, since $N(^2P_{J'',m''})/N(^2P_{J,m})$ is small. In previous alkali-metal Zeeman transition studies [14,16,20], Eq. (7) has been analyzed including only the first term in the denominator, leading to a linear scaling with pressure. Significant curvature is evident in Fig. 4 and the pressure-dependent denominator is required for the present analysis. Often the ratio $N(^2P_{J'',m''})/N(^2P_{J,m})$ in the multiple collision term is neglected or assumed to be approximately independent of pressure [28], yielding the functional form

$$\frac{N(^2P_{J',m'})}{N(^2P_{J,m})}=\frac{a[M]}{1+b[M]}, \tag{8}$$

where the fit parameter, $a=g\sigma(J,m\rightarrow J',m')/A(^2P_{J',m'}\rightarrow{}^2S)$, specifies the desired collisional cross sections in terms of the known radiative rates. Such fits are shown with the data in Fig. 4 and the resulting cross sections are reported in Tables II and III. The quoted error bounds reflect one standard deviation in the fit parameters. These statistical errors range from 5% to 15%, depending on the intensity of the relevant spectral feature. The combination of the weaker excitation of the $\Delta m=\pm1$ transitions to $^2P_{3/2}$ and slower rates for $\Delta J\neq0$ transitions prevented an accurate determination of the missing cross sections in Table II.

The primary source of systematic error is the detection of scattered laser light at the same wavelength as emission from the parent level. By temporarily reducing the magnetic field, the rubidium absorption feature was detuned from the laser excitation frequency and a fluorescence spectrum consisting of scattered light only was recorded. This scattered light signal was then subtracted from the rubidium emission spectrum [27]. The scattered laser light was most severe for the weaker excitation of $^2P_{3/2,\pm3/2}$. Uncertainty in this correction was typically <5% and always less than 15%.

The rare-gas data have been analyzed in Table III with certain constraints on the relative cross sections, as discussed below.

IV. DISCUSSION

A. Examination of detailed balancing, symmetry, and scaling relationships

The cross sections for nitrogen as reported in Table II obey the principle of detailed balancing:

$$\frac{\sigma(J,m\rightarrow J',m')}{\sigma(J',m'\rightarrow J,m)}=\left(\frac{g_J}{g_{J'}}\right)\exp\left(\frac{\varepsilon_{J,m}-\varepsilon_{J',m'}}{k_BT}\right). \tag{9}$$

The average detailed balancing ratio within a ^2P_J manifold reported in Table II is 0.98 ± 0.22, which compares favorably with the predicted value 0.98–0.99, depending on the size of Δm. Similarly for the cross sections involving $\Delta J\neq0$, the average observed detailed balancing ratio is 0.36 ± 0.03, compared to the predicted value of 0.36. The cross section for the transition $^2P_{3/2,-3/2}\rightarrow{}^2P_{3/2,1/2}$ is low relative to the

TABLE III. Cross sections for transitions between Zeeman-split Rb($^2P_{J,m}$) levels induced by collisions with rare gases, $\sigma(J,m\rightarrow J',m')$ (10^{-16} cm^2).

Transition	He	Ne	Ar	Kr	Xe
(3/2,1/2→3/2,−1/2)	34±4	50± 3	109±13	109±13	115±14
(1/2,1/2→1/2,−1/2)	16±1	24± 5	34± 5	34± 5	39± 4
(3/2,3/2→3/2,1/2)	64±7	150±26	248±23	248±23	224±28
(3/2,3/2→3/2,−1/2)	75±9	131±13	223±29	223±29	243±36

TABLE IV. Symmetry relationship of Eq. (10) observed for N_2 collisions $\sigma(J,m\rightarrow J,m')/\sigma(J,-m\rightarrow J,-m')$.

(J,m)	$m'=3/2$	$m'=1/2$	$m'=-1/2$	$m'=-3/2$
(3/2,3/2)		1.14 ± 0.17	1.10 ± 0.20	0.93 ± 0.21
(3/2,1/2)	1.10 ± 0.10		0.97 ± 0.05	1.03 ± 0.12

$^2P_{3/2,1/2}\rightarrow{}^2P_{3/2,-1/2}$ transition. However, the uncertainty in the observed values are also larger than typical.

Due to the small Zeeman splitting, it has been argued that a symmetry in the mixing cross sections,

$$\sigma(J,m\rightarrow J,m')=\sigma(J,-m\rightarrow J,-m'), \tag{10}$$

should be observed [17]. The cross sections observed for nitrogen obey this relationship, within the 5–15% error bounds, as demonstrated in Table IV. Similarly, the relationship

$$\sigma(J,m\rightarrow J',m)=\sigma(J,-m\rightarrow J',-m) \tag{11}$$

has been employed to relate multipole relaxation cross sections to the Zeeman mixing cross sections [20]. The cross sections for the $^2P_{3/2,1/2}\rightarrow{}^2P_{1/2,1/2}$ and $^2P_{3/2,-1/2}\rightarrow{}^2P_{1/2,-1/2}$ transitions are $(15\pm2)\times10^{-16}$ cm^2 and $(15\pm1)\times10^{-16}$ cm^2, and for the $^2P_{1/2,1/2}\rightarrow{}^2P_{3/2,1/2}$ and $^2P_{1/2,-1/2}\rightarrow{}^2P_{3/2,-1/2}$ transitions are $(5.0\pm0.2)\times10^{-16}$ cm^2 and $(4.9\pm0.2)\times10^{-16}$ cm^2, in very good agreement with Eq. (11).

The state-to-state Zeeman transition cross sections have been reported for the higher-lying Rb($6\,^2P$) levels for collisions with He, Ne, and Ar using pulsed excitation and a scanning Fabry-Pérot interferometer to resolve the fluorescence [20]. The reported cross sections exhibit significant deviations from the principle of detailed balancing, and the uncertainty in the observed cross sections of 20–50% is inadequate to provide a similar test of the symmetry relations (10) and (11).

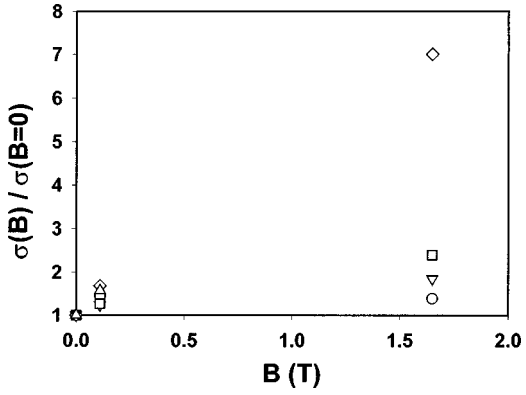

FIG. 5. Cross sections for transfer between Zeeman-split levels as a function of magnetic field strength: (○) Rb-He for $\sigma(1/2,-1/2\rightarrow1/2,1/2)$, (▽) Rb-Ar for $\sigma(1/2,-1/2\rightarrow1/2,1/2)$, (□) Rb-Kr for $\sigma(1/2,-1/2\rightarrow1/2,1/2)$, (◇) Rb-Ne for $\sigma(3/2,1/2\rightarrow3/2,-3/2)$, and (△) Rb-Ar for $\sigma(3/2,1/2\rightarrow3/2,-3/2)$. The data for 1.65 T are from the present work, for 0.11 T from Ref. [8] and for zero field from Refs. [4] and [6].

TABLE V. Comparison of observed and calculated multipole scaling relationships.

	Experiment		Theory	
Relative cross sections	N_2 (present)	(He) (Ref. [8])	(Ref. [29])	Ref. [30]
$\sigma^{(2)}_{3/2}/\sigma^{(1)}_{3/2}$	1.29 ± 0.16	1.25 ± 0.09	1.24	1.22
$\sigma^{(2)}_{3/2}/\sigma^{(3)}_{3/2}$	0.98 ± 0.10		1.13	1.12
$\sigma^{(3)}_{3/2}/\sigma^{(1)}_{3/2}$	1.31 ± 0.19		1.10	1.09

For the rare-gas collisions reported in Table III, the relations (9)–(11) have been employed in analyzing the data, and only the reduced set of independent cross sections are reported.

Scaling ratios have also been computed for multipole relaxation rates assuming no change in nuclear moment and a van der Waals collision interaction potential [29] (Table V). The data reported in Table II can be transformed to these cross sections for multipole relaxation using the relationship (11) to yield [20]

$$\sigma^{(1)}_{1/2}=2\sigma(1/2,1/2\rightarrow1/2,-1/2), \tag{12}$$

$$\begin{aligned}\sigma^{(1)}_{3/2}=&(1/5)\sigma(3/2,-1/2\rightarrow3/2,1/2)\\&+(8/5)\sigma(3/2,-3/2\rightarrow3/2,1/2)\\&+(9/5)\sigma(3/2,-3/2\rightarrow3/2,3/2)\\&+(2/5)\sigma(3/2,3/2\rightarrow3/2,1/2),\end{aligned} \tag{13}$$

$$\sigma^{(2)}_{3/2}=2\sigma(3/2,-3/2\rightarrow3/2,1/2)+2\sigma(3/2,3/2\rightarrow3/2,1/2), \tag{14}$$

$$\begin{aligned}\sigma^{(3)}_{3/2}=&(9/5)\sigma(3/2,-1/2\rightarrow3/2,1/2)\\&+(2/5)\sigma(3/2,-3/2\rightarrow3/2,1/2)\\&+(1/5)\sigma(3/2,-3/2\rightarrow3/2,3/2)\\&+(8/5)\sigma(3/2,3/2\rightarrow3/2,1/2).\end{aligned} \tag{15}$$

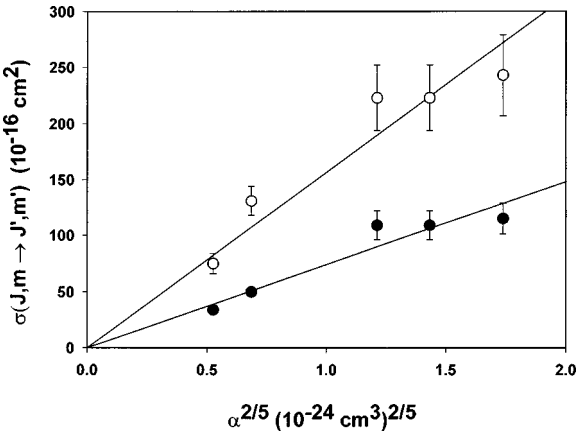

FIG. 6. Dependence of Zeeman transfer cross sections on polarizability for rare-gas collision partners: (○) $\sigma(3/2,3/2\rightarrow3/2,-1/2)$ and (●) $\sigma(3/2,1/2\rightarrow3/2,-1/2)$. A linear regression with zero intercept (—) is also shown for each case.

TABLE VI. Comparison of pressure broadening, Zeeman, and fine-structure mixing cross sections.

	$\sigma(10^{-16}\ \mathrm{cm}^2)\ {}^2P_{1/2}$			
Collision Partner, M	Pressure broadening	Zeeman $(1/2,1/2\rightarrow 1/2,-1/2)$	Fine structure	Quenching ${}^2P\rightarrow{}^2S$
He	52	16	0.072	
Ne	54	35	0.0014	
Ar	134	24	0.00051	
Kr	157	34	0.00036	
Xe	189	39	0.00034	
H_2	34		10.	6
D_2	39		21.4	3
N_2	106	33	13.2	58
CH_4	151		29.5	<1
CF_4	174		9.5	
	$\sigma(10^{-16}\ \mathrm{cm}^2)\ {}^2P_{3/2}$			
Collision partner, M	Pressure Broadening	Zeeman $(3/2,1/2\rightarrow 3/2,-1/2)$	Zeeman (mean)	Fine structure	Quenching ${}^2P\rightarrow{}^2S$
He	55	34	58	0.105	
Ne	54	50	114	0.0022	
Ar	130	57	113	0.00073	
Kr	158	109	193	0.00045	
Xe	189	115	194	0.00049	
H_2	34			13.9	3
D_2	39			29.8	5
N_2	106	59	74	18.4	43
CH_4	151			41.0	3
CF_4	174			13.2	

The ratio of misalignment to disorientation cross sections, $\sigma^{(2)}_{3/2}/\sigma^{(1)}_{3/2}$, using the present nitrogen data, is 1.29 ± 0.16, which agrees favorably with a previous observation for Rb($5\,{}^2P$)-He of 1.25 ± 0.09 and similar values for other rare-gas collision partners [8]. Several theoretical predictions for this ratio have been reported as 1.15–1.73 [29–34]. The cross section $\sigma^{(3)}_{3/2}$ is usually not determined from depolarization experiments [8], but may be computed from the current N_2 data as $\sigma^{(3)}_{3/2}=(259\pm15)\times10^{-16}$ cm^2. This result is 15–20% larger than the value predicted theoretically from the ratios $\sigma^{(2)}_{3/2}/\sigma^{(3)}_{3/2}=1.12$ and $\sigma^{(3)}_{3/2}/\sigma^{(1)}_{3/2}=1.09$ [29,30].

B. Magnetic-field dependence

The cross sections for multipole relaxation of Rb($5\,{}^2P$) for rare-gas collisions have been reported previously for low magnetic fields [4,6,8]. Magnetic-field-induced ${}^2P_{1/2}$-${}^2P_{3/2}$ mixing can enhance the Zeeman mixing rates, and a significant dependence on magnetic field strength has been observed for Cs and other alkali metals [21]. To place the current work in context of the previously measured values of disorientation and misalignment cross sections, a plot of several m-specific cross sections for rare-gas collisions as a function of field strength is shown in Fig. 5. The cross section for helium, $\sigma(1/2,1/2\rightarrow1/2,-1/2)$, shows little dependence on field strength. Recent measurements and predictions of this particular cross section also exhibit no dependence on field strength in the range 1–7 T [21]. However, Kedzierski *et al.* [21] report an absolute value for this cross section of 5.8×10^{-16} cm^2, which is significantly less than values shown in Fig. 5 of $(11.5–16.6)\times10^{-16}$ cm^2. The cross sections exhibit a considerably stronger dependence on magnetic field for higher mass rare-gas collision partners, and for transitions within the ${}^2P_{3/2}$ manifold.

C. Rare-gas collision partners

The cross sections for transitions between Zeeman-split levels depend on the polarizability of the rare-gas collision partner as shown in Fig. 6. These results are in good agreement with the calculations of Gordeyev *et al.*, who predict for large fine-structure splitting (adiabatic conditions) [33]

$$\sigma(3/2,1/2\rightarrow3/2,-1/2)=0.226\left(\frac{\alpha e^2\langle r^2\rangle}{h\nu/2\pi}\right)^{2/5}, \qquad (16)$$

$$\sigma(3/2,3/2\rightarrow3/2,-1/2)=0.540\left(\frac{\alpha e^2\langle r^2\rangle}{h\nu/2\pi}\right)^{2/5}, \qquad (17)$$

where α is the polarizability of the rare-gas collision partner, $\langle r^2\rangle$ is the average radius of the valence electron orbit squared, and ν is the relative speed of collision pair.

A linear fit of the data in Fig. 6 provides a ratio of slopes for the $\sigma(3/2,3/2\rightarrow3/2,-1/2)$ and $\sigma(3/2,1/2\rightarrow3/2,-1/2)$ cross sections of 2.17 ± 0.19, which agrees favorably with the ratio of 2.39 predicted by Eqs. (16) and (17).

The current studies were performed in conjunction with pressure broadening, fine-structure mixing, and quenching studies of Rb($5\,^2P$), which are summarized in Table VI [22,35]. Typically, the cross sections for dephasing collisions (pressure broadening) are the largest. However, the rates for transitions between the Zeeman-split $^2P_{3/2}$ levels are often as large as, and sometimes exceed, the pressure broadening rates. While cross sections for specific transitions between Zeeman levels, particularly the $\sigma(3/2,3/2\rightarrow 3/2,1/2)$ and $\sigma(3/2,3/2\rightarrow 3/2,-1/2)$, are large, the average cross sections for the $^2P_{3/2}$ manifold are closer to the pressure broadening values. In addition, the pressure broadening rates were determined for no applied magnetic field, and the large Zeeman transfer rates may reflect the increase in cross section with magnetic field as shown in Fig. 5. It would be interesting to investigate the influence of magnetic field on pressure-induced line broadening. Regardless, the cross sections for transitions between (J,m) levels are very large and inelastic collision contribute significantly to the broadening mechanism.

V. CONCLUSIONS

Steady-state, spectrally resolved laser-induced fluorescence techniques have been used to determine state-to-state cross sections, $\sigma(J,m\rightarrow J',m')$, for collision-induced transitions between the six Zeeman-split sublevels of Rb($5\,^2P$). These levels are very strongly coupled, yet the transfer rates exhibit a significant dependence on initial and final (J,m) states, in accordance with theoretical symmetry and scaling predictions. The Zeeman transition cross sections are typically as large as the corresponding pressure broadening cross sections. While the fine-structure splitting is slightly larger than the average kinetic energy, mixing between states of different J is significant for the molecular collision partner N_2. For rare-gas collision partners the cross sections scale with polarizability, as expected.

[1] E. E. Nikitin, in *The Excited State in Chemical Physics*, edited by J. W. McGowan (John Wiley and Sons, New York, 1975).
[2] W. E. Baylis, in *Progress in Atomic Spectroscopy, Part B*, edited by W. Hanle and H. Kleinpoppen (Plenum, New York, 1978).
[3] E. P. Gordeyev, E. E. Nikitin, and M. Ya. Ovchinnikova, Can. J. Phys. **47**, 1819 (1969).
[4] A. Gallagher, Phys. Rev. **157**, 68 (1961).
[5] W. Berdowski, T. Shiner, and L. Krause, Phys. Rev. A **4**, 984 (1971).
[6] B. R. Bulos and W. Happer, Phys. Rev. A **4**, 849 (1971).
[7] J. Guiry and L. Krause, Phys. Rev. A **12**, 2407 (1975).
[8] B. Kamke, Z. Phys. A **273**, 23 (1975).
[9] H. Doebler and B. Kamke, Z. Phys. A **280**, 111 (1977).
[10] B. Brouillaud and R. Gayet, J. Phys. B **10**, 2143 (1977).
[11] A. Sieradzan and F. A. Franz, Phys. Rev. A **25**, 2985 (1982).
[12] R. W. Berends, P. Skalinski, and L. Krause, J. Phys. B **17**, 605 (1984).
[13] X. L. Han and G. W. Schinn, Phys. Rev. A **43**, 266 (1991).
[14] J. C. Gay and W. B. Schneider, Z. Phys. A **278**, 211 (1976).
[15] J. C. Gay and W. B. Schneider, Phys. Rev. A **20**, 905 (1979).
[16] R. Boggy and F. A. Franz, Phys. Rev. A **25**, 1887 (1982).
[17] P. Skalinski and L. Krause, Phys. Rev. A **26**, 3338 (1982).
[18] R. W. Berends, W. Kedzierski, and L. Krause, Phys. Rev. A **37**, 68 (1988).
[19] R. W. Berends, W. Kedzierski, W. E. Baylis, and L. Krause, Phys. Rev. A **39**, 1526 (1989).
[20] W. Kedzierski, R. B. Middleton, and L. Krause, Phys. Rev. A **43**, 143 (1991).
[21] W. Kedzierski, Ju Gao, W. E. Baylis, and L. Krause, Phys. Rev. A **49**, 4540 (1994).
[22] M. D. Rotondaro and G. P. Perram (unpublished).
[23] L. Krause, Appl. Opt. **5**, 1375 (1966).
[24] A. Gallagher, Phys. Rev. **172**, 88 (1968).
[25] J. K. Link, J. Opt. Soc. Am. **56**, 1195 (1966).
[26] H. E. White, *Introduction to Atomic Spectra* (McGraw Hill, New York, 1934).
[27] M. D. Rotondaro (unpublished).
[28] G. P. Perram, D. A. Massman, and S. J. Davis, J. Chem. Phys. **99**, 6634 (1993).
[29] A. I. Okunevich and V. I. Perel, Zh. Eksp. Teor. Fiz. **58**, 666 (1970) [Sov. Phys. JETP **31**, 356 (1970)].
[30] E. Roueff and A. Suzor, J. Phys. (France) **35**, 727 (1974).
[31] E. I. Dashevskaya and N. A. Mochova, Opt. Spectrosc. **33**, 817 (1972).
[32] F. H. Mies, Phys. Rev. A **7**, 942 (1973).
[33] E. P. Gordeyev, E. E. Nikitin, and M. Ya. Ovchinnikova, Can. J. Phys. **47**, 1819 (1969).
[34] M. Elbel, Phys. Lett. **28A**, 4 (1968).
[35] M. D. Rotondaro and G. P. Perram, J. Quant. Spectrosc. Radiat. Transf. **57**, 497 (1997).